

# Image Reconstruction by the Method of Convex Projections

Tomohiro Aoyagi\*, Kouichi Ohtsubo and Nobuo Aoyagi  
*Faculty of Information Sciences and Arts, Toyo University, 2100 Kujirai, Saitama, Japan*

Keywords: Computerized Tomography, Convex Projection, Closed Convex Set.

Abstract: In medical imaging modality, such as X-ray computerized tomography (CT) and positron emission tomography (PET), image reconstruction from projection is to produce an image of a two dimensional object from its line integrals along a finite number of lines. Given some subsets of a priori knowledge about the problem in Hilbert space, a formalized problem is to find the object from observed vector. If the subsets are closed and convex sets, given the convex projections onto the sets, the problem can be solved by using the method of projections onto convex sets (POCS). In this paper, we apply the method of projection onto convex sets to image reconstruction problems and evaluate the image quality in computer simulations. Also, we evaluate the influence of the noise in reconstructed image.

## 1 INTRODUCTION

In medical imaging modality, such as X-ray computerized tomography (CT) and positron emission tomography (PET), image reconstruction from projection is to produce an image of a two dimensional object from estimates of its line integrals along a finite number of lines of known locations (Herman, 2009; Kak et al., 1998; Imimy, 1985). If  $g(y)$  is an observed function,  $K(x, y)$  is a known kernel and  $f(x)$  is unknown function or object to be determined, then image reconstruction problem can be formulated by

$$g(y) = \int_a^b K(x, y)f(x) dx.$$

This is known as a Fredholm integral equation of the first kind. Because of the ill-posed nature, it is difficult to solve strictly this integral equation. Since observed function can be discretized experimentally, it is necessary to discretize the integral kernel and object to solve it in computer. This leads to the problem of seeking the inverse of some matrix (Bertero et al., 1985; Bertero et al., 1988). In finite dimensional vector space, if an observed data is a vector in  $N$  dimensional space and an object data is a vector in  $M$  dimensional space, the integral kernel can be expressed by  $N \times M$  matrix. If  $N = M$  and the

matrix is nonsingular, there exist an inverse. Then, object vector to be reconstructed can be obtain by using observed vector and an inverse. However, in general, because the matrix is not always nonsingular, there is no guarantee of existence and uniqueness for the solution. Given some subsets of a priori knowledge about the problem in Hilbert space, a formalized problem is to find the object or element  $f$  from observed vector. If the subsets are closed and convex sets, given the convex projections onto the sets, the problem can be solved by using the method of projections onto convex sets (POCS) (Stark et al., 1998). POCS is an iterative algorithm for solving a Fredholm equation of the first kind. Up to now it has been used in CT, electron microscope, pattern recognition, phase retrieval, image compression, image restoration and so on (Sezan et al., 1984; Sezan et al., 1982; Oskoui-fard et al., 1988; Kudo et al., 1991; Bauschke et al., 2003). Algebraic reconstruction techniques (ART) is also one of POCS for solving a system of simultaneous equation. In this paper, we apply the method of projection onto convex sets to image reconstruction problems and evaluate the image quality in computer simulations. Also, we evaluate the influence of the noise in reconstructed image.

\* <https://www.toyo.ac.jp/>

## 2 IMAGE RECONSTRUCTION FROM PROJECTIONS

Let us consider the problem of computerized tomography that is to reconstruct an object on the orthogonal coordinate system of 2 dimensional Euclidean space  $\mathbb{R}^2$ . Let  $(x, y)$  be the orthogonal coordinates of any point in the plane. Let  $(X, Y)$  be the orthogonal coordinates of any point which are rotated through  $\theta$  degrees around the origin. And, let  $f(x, y)$  be an object which is, for example, X-ray absorption coefficient or the distribution of the nuclide. For this setting, we can define the integral of the function  $f(x, y)$  along  $\theta$  direction, such that,

$$g(X, \theta) = \int_{-\infty}^{\infty} f(x, y) dY. \quad (2)$$

This is known as a parallel projection, the ray-sum of  $f(x, y)$ , the Radon transform or the X-ray transform. Figure 1 shows an object, its coordinate system and a parallel projection. The real problem in CT is to reconstruct  $f$  from a finite number of its line integrals, and the reconstruction procedure has to be adapted to the scanning geometry. The settings of finite sampling and scanning geometry on resolution and accuracy is one of the main problems in CT (Natterer, 2001).

## 3 THE METHOD OF CONVEX PROJECTIONS

Assume that  $C_1, C_2, \dots, C_m$  denote  $m$  closed convex sets in Hilbert space  $H$ , and  $C_0$  denotes their intersection set.

$$C_0 = \bigcap_{i=1}^m C_i. \quad (3)$$

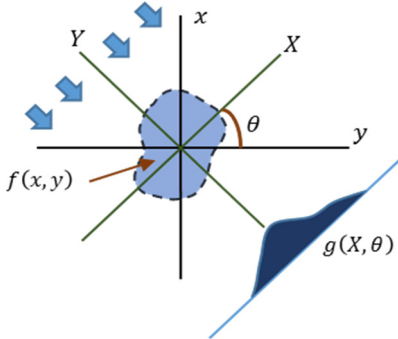


Figure 1: An object,  $f(x, y)$ , and its projection,  $g(X, \theta)$ , are shown for an angle of  $\theta$ .

For each  $i = 1, 2, \dots, m$ , let  $P_i$  denote the projection operator onto the set  $C_i$ , and  $T_i$  denote the corresponding relaxed projector, such that,

$$T_i = I + \lambda_i(P_i - I), \lambda_i \in (0, 2). \quad (4)$$

The  $\lambda_i$  are called relaxation parameters, and can be adjusted to accelerate the rate of convergence. Moreover, we define the composition of the relaxed projectors.

$$T = T_m T_{m-1} \dots T_1. \quad (5)$$

Then, we have the following theorem.

**Theorem** (Fundamental Theorem of POCS).

Assume that  $C_0$  is non-empty. Then for every  $x \in H$  and for every  $\lambda_i \in (0, 2), i = 1, 2, \dots, m$ , the sequence  $\{T^n x\}$  converges weakly to a point of  $C_0$ .

This theorem was proved with the fixed point theorem of non-expansive mappings by Youla et al. in 1982 (Youla et al., 1982). In a finite dimensional vector space, the sequence  $\{T^n x\}$  converges strongly to  $x \in C_0$  (Takahashi, 2000).

Constraint sets used by this paper are listed below.

The derivation of the projection operators is given in (Youla et al., 1982).

$$1) C_\alpha = \{f: f \in \mathcal{H}, f(x, y) = 0 \text{ for } (x, y) \notin D\}. \quad (6)$$

In other words,  $C_\alpha$  is the set of all functions in  $H$  that are spatially band-limited in finite region  $D$ . In short, it is compact support. The projection  $P_\alpha$  onto  $C_\alpha$  is given by

$$P_\alpha f(x, y) = \begin{cases} f(x, y) & (x, y) \in D \\ 0 & (x, y) \notin D \end{cases}. \quad (7)$$

$$2) C_\beta = \left\{ \begin{array}{l} f: f \in \mathcal{H}, f(x, y) \geq 0 \\ \text{for all } (x, y) \in D \end{array} \right\}. \quad (8)$$

In other words,  $C_\beta$  is the set of all function in  $H$  that are nonnegative. The projection  $P_\beta$  onto  $C_\beta$  is given by

$$P_\beta f(x, y) = \begin{cases} f(x, y) & \text{if } f \geq 0 \\ 0 & \text{if } f < 0 \end{cases}. \quad (9)$$

$$3) C_\gamma = \{f: f \in \mathcal{H}, a \leq f(x, y) \leq b\}. \quad (10)$$

In other words,  $C_\gamma$  is the set of all function in  $H$  that are amplitude-limited in the range  $[a, b]$ . The projection  $P_\gamma$  onto  $C_\gamma$  is given by

$$P_\gamma f(x, y) = \begin{cases} a & f(x, y) < a \\ f(x, y) & a \leq f(x, y) \leq b. \\ b & f(x, y) > b \end{cases}. \quad (11)$$

Let us consider the set that are obtained by the line integral. It is inner product in Hilbert space  $H$ , that is,

$$C = \{f: \langle f, a \rangle = b\}. \quad (12)$$

Let  $g_1, g_2 \in C$ ,  $g_3 = \alpha g_1 + (1 - \alpha)g_2$ , for  $\alpha \in [0, 1]$ . Then,

$$\begin{aligned} \langle g_3, a \rangle &= \langle \alpha g_1 + (1 - \alpha)g_2, a \rangle \\ &= \alpha \langle g_1, a \rangle + (1 - \alpha) \langle g_2, a \rangle \\ &= \alpha b + (1 - \alpha)b = b. \end{aligned} \quad (13)$$

Hence,  $g_3 \in C$  and  $C$  is convex.

Next, let  $\{f_k\}$  be a sequence in  $C$  such that  $f_k \rightarrow f^*$ . By the Schwarz inequality, we obtain

$$\begin{aligned} |\langle f_k, a \rangle - \langle f^*, a \rangle| &= |\langle f_k - f^*, a \rangle| \\ &\leq \|f_k - f^*\| \cdot \|a\| \rightarrow 0. \end{aligned} \quad (14)$$

Thus,

$$\langle f^*, a \rangle = \lim_{k \rightarrow \infty} \langle f_k, a \rangle = b. \quad (15)$$

Hence,  $f^* \in C$  and set  $C$  is closed. Therefore,  $C$  is closed convex set.

The projection of an arbitrary  $x$  onto the set  $C$  is driven. We need to find a  $y \in C$ , for an arbitrary  $x \in H$ , that minimizes  $\|y - x\|$ . Let  $a_0 = a/\|a\|$ . Then, each vector  $x \in H$  has the following orthogonal decomposition, that is,

$$x = \langle x, a_0 \rangle a_0 + d. \quad (16)$$

Hence,

$$d = x - \langle x, a_0 \rangle a_0. \quad (17)$$

Clearly  $\langle d, a_0 \rangle = 0$  so  $d$  is orthogonal to  $a_0$ . Since each  $y \in C$  satisfies  $\langle y, a \rangle = b$ , i.e.,  $\langle y, a_0 \rangle = b/\|a\|$ , we can write  $y$  according to eq. (16) as

$$y = \frac{b}{\|a\|} a_0 + e, \quad (18)$$

where  $e$  is a vector that is orthogonal to  $a_0$ .

Let us consider  $x \notin C$  and  $y \in C$ . From eq. (16) and (18) we have

$$\begin{aligned} \|x - y\|^2 &= \left\| \langle x, a_0 \rangle a_0 + d - \left( \frac{b}{\|a\|} a_0 + e \right) \right\|^2 \\ &= \left\| \left( \langle x, a_0 \rangle - \frac{b}{\|a\|} \right) a_0 + (d - e) \right\|^2 \end{aligned} \quad (19)$$

Since  $a_0$  is orthogonal to  $d - e$ ,  $\langle a_0, d - e \rangle = 0$ .

Then, we write

$$\begin{aligned} \|x - y\|^2 &= \left\| \left( \langle x, a_0 \rangle - \frac{b}{\|a\|} \right) a_0 \right\|^2 + \|d - e\|^2. \end{aligned} \quad (20)$$

We need to minimize  $\|x - y\|^2$ . Since  $\|d - e\|^2 = 0$ ,  $d = e$ . From eq. (18), we can write

$$\begin{aligned} y &= \frac{b}{\|a\|} a_0 + d \\ &= \frac{b}{\|a\|} a_0 + x - \langle x, a_0 \rangle a_0 \\ &= x + \left( \frac{b}{\|a\|} - \langle x, a_0 \rangle \right) a_0 \\ &= x + \frac{b - \langle x, a \rangle}{\|a\|^2} a. \end{aligned} \quad (21)$$

We conclude that

$$y = x + \frac{b - \langle x, a \rangle}{\|a\|^2} a, \quad (22)$$

which is the projection of  $x$  onto the set  $C$ .

## 4 COMPUTER SIMULATIONS

To confirm the effectiveness of the method, computer simulations were carried out. A Cartesian grid of the square observation plane, called pixels, is introduced into the region of interest (ROI) so that it covers the whole observation plane that has to be reconstructed. The pixels are numbered in some manner. We set the top left corner pixel 1 and bottom right corner pixel  $M$  with Raster scanning. The object to be reconstructed is approximated by one that takes a constant uniform value  $f_j$  throughout the  $j$ -th pixel, for  $j = 1, 2, \dots, M$ .

Thus the vector  $\mathbf{f} = \{f_j\}_{j=1}^M$  in  $\mathbb{R}^M$  is the discretized version of the object (Censor et al., 2008).

For our simulations we assumed the parallel mode of data collection. The set of all lines for which line integrals are estimated is divided into  $V$  sets of  $N/V$  lines in each. The lines within a set are parallel and equidistant. The total number of all discretized line is  $N$ . We assumed projection angle  $\theta = [0, \pi]$ , and it is discretized at even. We set the left detector element to 1 at  $\theta = 0$  and the right detector element to  $N$  at last View. Thus  $i$  indicates any detector elements and  $i = 1, 2, \dots, N$ . We denote the length of intersection of the  $i$ -th line with the  $j$ -th pixel by  $a_j^i$ , for all  $i = 1, 2, \dots, N$ ,  $j = 1, 2, \dots, M$ . Therefore, in this model, each line integral is approximated by a finite sum and represented by a system of linear equations, such that,

$$\sum_{j=1}^M a_j^i f_j = g_i, i = 1, 2, \dots, N. \quad (23)$$

Thus the vector  $\mathbf{g} = \{g_i\}_{i=1}^N$  in  $\mathbb{R}^N$  is the discretized version of the line integral or parallel projection. Using vector notation, it can be expressed by

$$\mathbf{g} = \mathbf{A}\mathbf{f}. \quad (24)$$

Figure 2 shows the discretized model of the image reconstruction problem.

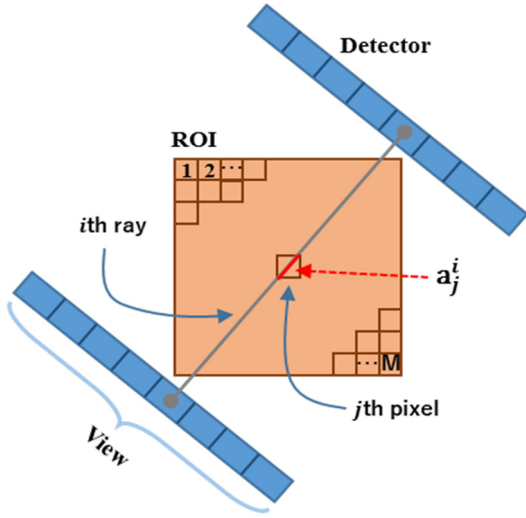


Figure 2: The fully-discretized model of the image reconstruction problem.



Figure 3: The original test image 1 (128x128pixel, 8bpp) and its projection data (Sinogram: 128 Detectors, 100 Views and 8bpp).



Figure 4: The reconstruction image using FBP.

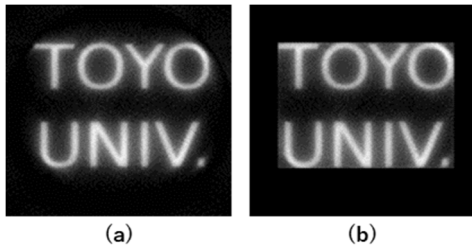


Figure 5: The reconstructed image using (a) ART (10 iterations), (b) ART with  $P_\alpha, P_\beta$  and  $P_\gamma$  (10 iterations).

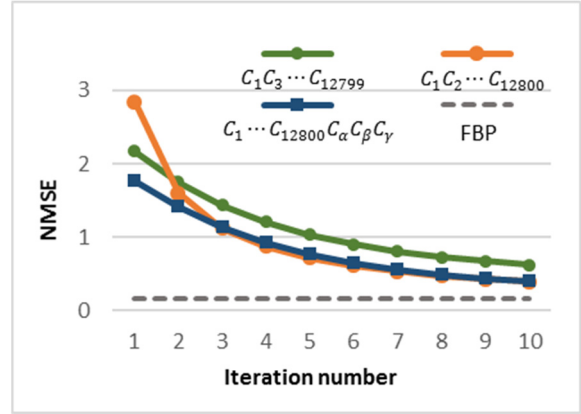


Figure 6: Plots of the normalized mean square error versus iteration number.

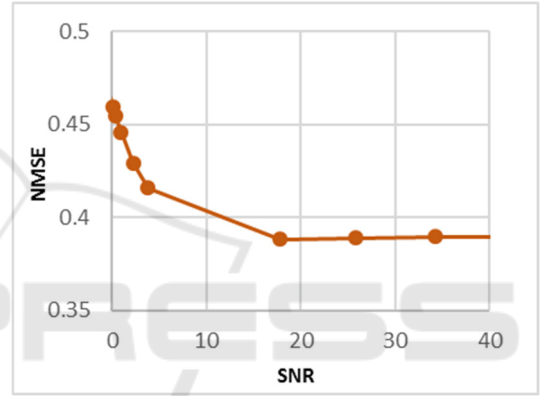


Figure 7: Plot of the normalized mean square error versus SNR.

The ART is the following iterative scheme.

Algorithm.

Step 1 (Initialization):  $\mathbf{f}^0 \in \mathbb{R}^M$  and the relaxation parameter  $\lambda_k$  is arbitrary.

Step 2 (Iterative Step): Given  $\mathbf{f}^k$  compute

$$\mathbf{f}^{k+1} = \mathbf{f}^k + \lambda_k \frac{\mathbf{g}_i - \langle \mathbf{a}^i, \mathbf{f}^k \rangle}{\|\mathbf{a}^i\|_2^2} \mathbf{a}^i, \quad (25)$$

where  $k \in \mathbb{Z}_{\geq 0}$  and  $\lambda_k \in (0, 2)$ .  $\|\cdot\|_2$  indicates the  $\ell^2$ -norm.

$$\langle \mathbf{a}^i, \mathbf{f}^k \rangle = \sum_{j=1}^M a_j^i f_j^k. \quad (26)$$

Having identified the ART as convex projection algorithm, we can describe the ART algorithm by

$$\mathbf{f}^{k+1} = P_{\text{ART}} \mathbf{f}^k, \quad (27)$$

where  $P_{\text{ART}}$  is defined as following.

$$P_{\text{ART}} = P_N \cdots P_2 P_1. \quad (28)$$

It means that  $P_{ART}$  is constituted by a composition of  $N$  projection operators  $P_i$  that project onto the closed convex sets  $C_i, i = 1, 2, \dots, N$ .

Our first image is a text based phantom. Figure 3 shows its original test image, discretized  $128 \times 128$  pixels, and its parallel projection data, called sinogram. In this case we set 100 projections with 128 line per projection. The sinogram is shown  $128 \times 100$  pixels. Figure 4 shows the reconstructed image with the filtered backprojection algorithm (FBP) for reference. FBP is an important reconstruction algorithm in tomography. It can be viewed as a numerical implementation of the inversion formula of the Radon transform. Figure 5 shows the reconstructed image with the method of convex projections after 10 iterations. Fig.5 (a) is the reconstructed image by ART without a priori constraints. It can be written as

$$\mathbf{f}^{k+1} = P_N \dots P_2 P_1 \mathbf{f}^k. \quad (29)$$

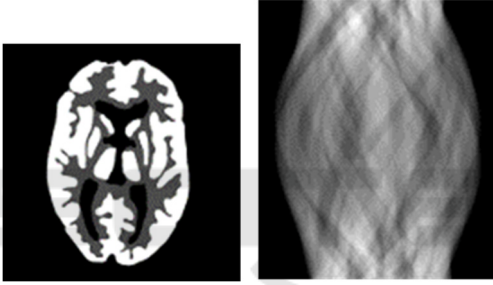


Figure 8: The original test image 2 ( $128 \times 128$  pixel, 8bpp) and its projection data (Sinogram: 128 Detectors, 150 Views and 8bpp.)

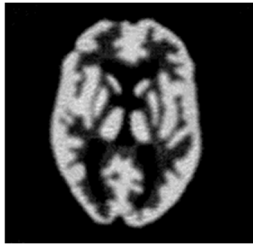


Figure 9: The reconstruction image using FBP.

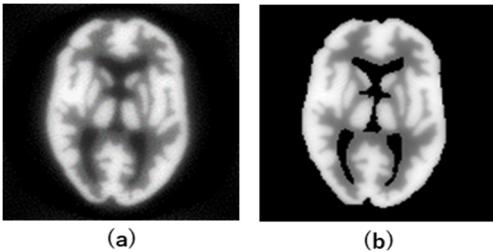


Figure 10: The reconstructed image using (a) ART (10 iterations), (b) ART with  $P_\alpha, P_\beta$  and  $P_\gamma$  (10 iterations).

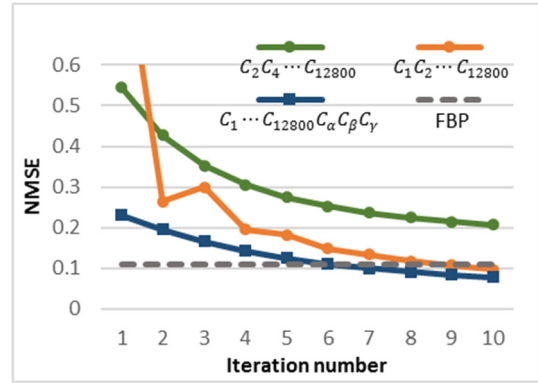


Figure 11: Plots of the normalized mean square error versus iteration number.

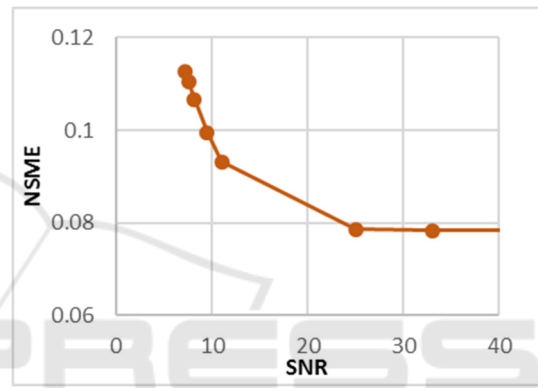


Figure 12: Plot of the normalized mean square error versus SNR.

Fig. 5 (b) is the reconstructed image by ART with three prior constraints. It can be written as

$$\mathbf{f}^{k+1} = P_\gamma P_\beta P_\alpha P_N \dots P_2 P_1 \mathbf{f}^k. \quad (30)$$

In this case we set the starting data to the origin,  $0 = \mathbf{f}^0 \in \mathbb{R}^M$ , and the relaxation parameter  $\lambda_k$  to 0.01.

Figure 6 illustrates the plots of the normalized mean square error versus iteration number to compare the error of the reconstruction. The normalized mean square error is defined by

$$NMSE(k) = \frac{\|\mathbf{f}^k - \mathbf{f}\|_2^2}{\|\mathbf{f}\|_2^2}, \quad (31)$$

where  $\mathbf{f}^k$  is the image after  $k$ 'th iteration step and  $\mathbf{f}$  is the original image. In Fig. 6 the green line shows the NMSE by using the convex projections  $P_{12799} P_{12797} \dots P_3 P_1$ . The reconstruction was updated by

$$\mathbf{f}^{k+1} = P_{12799} P_{12797} \dots P_3 P_1 \mathbf{f}^k. \quad (32)$$

The total number of tis projections is 6400. The orange line shows the NMSE by using the convex projections

$P_{12800}P_{12799} \cdots P_2P_1$ . The reconstruction was updated by

$$\mathbf{f}^{k+1} = P_{12800}P_{12799} \cdots P_2P_1\mathbf{f}^k. \quad (33)$$

The total number of tis projections is 12800. The blue line shows the NMSE by using the convex projections  $P_\gamma P_\beta P_\alpha P_{12800} \cdots P_2P_1$ . The gray dotted line shows the NMSE by FBP for reference. From Fig. 6 we can see that the error decreases with increasing the number of projections and the number of iterations.

To confirm the influence of the noise, noises are added the projection data. Using vector notation, it can be expressed by

$$\mathbf{g} = \mathbf{A}\mathbf{f} + \mathbf{q}, \quad (34)$$

where  $\mathbf{q}$  indicates noise and is a normally distributed deviate with zero mean and unit variance (Press et al., 1992).

To measure the effect of noise on the reconstruction images, we use the signal-to-noise ratio (SNR) (Trussel, 2008). This is usually defined as the ratio of signal power  $\sigma_g^2$ , to noise power  $\sigma_q^2$ ,

$$\text{SNR} = \frac{\sigma_g^2}{\sigma_q^2}, \quad (35)$$

and in decibels

$$\text{SNR}_{\text{dB}} = 10 \times \log_{10} \left( \frac{\sigma_g^2}{\sigma_q^2} \right). \quad (36)$$

In projection data, the function power is usually estimated by the simple summation

$$\sigma_g^2 = \frac{1}{128 \times 100} \sum_{i=1}^{128 \times 100} \{g_i - \mu_g\}^2, \quad (37)$$

where  $\mu_g$  is the mean of the projection data.

Figure 7 illustrates the plots of the normalized mean square error versus SNR. From Fig. 7 we can see that the error decreases with increasing SNR.

Our second image is 2-dimensional numerical phantom which is modeled on Hoffmann brain phantom. Figure 8 shows its test image 2, discretized  $128 \times 128$  pixels, and its parallel projection data. In this case we set 150 projections with 128 line per projection. The sinogram is shown  $128 \times 150$  pixels. Figure 9 shows the reconstructed image with FBP for reference. Figure 10 shows the reconstructed image with the method of convex projections after 10 iterations. Fig.10 (a) is the reconstructed image by ART without a priori constraints. Fig.10 (b) is that with three prior constraints. Figure 11 illustrates the plots of the normalized mean square error versus iteration number with test image 2. In Fig. 11 the green line shows the NMSE by using the convex

projections  $P_{19200}P_{19198} \cdots P_4P_2$ . The reconstruction was updated by

$$\mathbf{f}^{k+1} = P_{19200}P_{19198} \cdots P_4P_2\mathbf{f}^k. \quad (38)$$

The total number of tis projections is 9600. The orange line shows the NMSE by using the convex projections  $P_{19200}P_{19199} \cdots P_2P_1$ . The total number of tis projections is 19200. The blue line shows the NMSE by using the convex projections  $P_\gamma P_\beta P_\alpha P_{19200} \cdots P_2P_1$ . The gray dotted line shows the NMSE by FBP for reference. From Fig. 11 we can see that the error decreases with increasing the number of projections and the number of iterations. Figure 12 illustrates the plots of the normalized mean square error versus SNR with the test image 2. From Fig. 12 we can see that the error decreases with increasing SNR.

## 5 CONCLUSIONS

By discretizing the image reconstruction problem, we applied the method of projection onto convex sets to the problem and evaluated the image quality. Also, we evaluated the influence of the noise in reconstructed image. We showed that the error decreases with increasing the number of projections and the number of iterations. Also, we showed that the error decreases with increasing SNR. However, by increasing the number of the projections and the iteration step, time consuming problem arise. And, by increasing the pixel size of object and the data size of sinogram, this method requires more computational time. If we get more priori information with respect to an object, this method can decrease the normalized mean square error in comparison to FBP.

In this study, there are many prior constraints except for our constraints used. If prior constraints are closed and convex set, these sets can be incorporated in this method. Therefore, it is necessary to create mathematically the subset in Hilbert space. Moreover, there are many parameters, such as initial data, the relaxation parameter and the pixel size of reconstructed image. The image quality of reconstructed image and the speed of the convergence in this method are affected by these. It is necessary to find the optimal parameters. These become the future problems.

## REFERENCES

- Herman, G., 2009. Fundamentals of Computerized Tomography, Springer-Verlag. London, 2<sup>nd</sup> edition.

- Kak, A., Slaney, M., 1988. Principles of computerized tomographic imaging, IEEE Press. New York.
- Imiya, A., 1985. A direct method of three dimensional image reconstruction from incomplete projection, Dr. Thesis, *Tokyo Institute of Technology*, Tokyo. (in Japanese)
- Bertero, M., Mol, C., Pike, E., 1985. Linear inverse problems with discrete data. I: General formulation and singular system analysis, *Inverse Problems*, 1, pp.301-330.
- Bertero, M., Mol, C., Pike, E., 1988. Linear inverse problems with discrete data: II. Stability and regularization", *Inverse Problems*, 4, pp.573-594.
- Stark, H., Yang, Y., 1998. Vector Space Projection, *John Wiley & Sons Inc. NY*.
- Sezan, M., Stark, H., 1984. Tomographic image reconstruction from incomplete view data by convex projections and direct Fourier inversion, *IEEE Trans. Med. Imaging*, 3, pp. 91-98.
- Sezan, M., Stark, H., 1982. Image restoration by the method of convex projections: part 2-applications and numerical results, *IEEE Trans. Med. Imaging*, 1, pp.95-101.
- Oskoui-fard, P., Stark, H., 1988. Tomographic image reconstruction using the theory of convex projections, *IEEE Trans. Med. Imaging*, 7, pp.45-58.
- Kudo, H., Saito, T., 1991. Sinogram recovery with the method of convex projections for limited-data reconstruction in computed tomography, *J. Opt. Soc. Am. A*, 8, pp. 1148-1160.
- Bauschke, H., Combettes, P., Luke, D., 2003. Hybrid projection-refraction method for phase retrieval, *J. Opt. Soc. Am. A*, 20, pp.1025-1034.
- Natterer, F., 2001. The Mathematics of Computerized Tomography, *SIAM*. Philadelphia.
- Youla, D., Webb, H., 1982. Image restoration by the method of convex projections: part 1-theory, *IEEE Trans. Med. Imaging*, 1, pp.81-94.
- Takahashi, W., 2000. Nonlinear Functional Analysis, *Yokohama Publishers, Inc.* Yokohama.
- Censor, Y., Elfving, T., Herman, G., Nikazad, T., 2008. On diagonally-relaxed orthogonal projection methods, *SIAM J. Sci. Comput.* 30, pp.473-504.
- Press, W., Teukolsky, S., Vetterling, W., Flannery, B., 1992. Numerical Recipes in C, *Cambridge University Press*. Cambridge, 2<sup>nd</sup> edition.
- Trussel, H., Vrhel, M., 2008. Fundamentals of Digital Imaging, *Cambridge University Press*. Cambridge.
- Simmons, G., 1963. Topology and Modern Analysis, *McGraw-Hill Inc. Singapore*.
- Wouk, A., 1979. A Course of Applied Functional Analysis, *John Wiley & Sons Inc. NY*.

#### Definition A.

Let  $H$  be an arbitrary Hilbert space. A convex set in  $H$  is a non-empty subset  $S$  with the property that if  $x$  and  $y$  are in  $S$ , then

$$z = x + t(y - x) = (1 - t)x + ty$$

is also in  $S$  for every real number  $t$  such that  $0 \leq t \leq 1$ .

#### Definition B.

A subset  $S$  of metric space  $X$  is called a closed set if it contains each of its limit points.

#### Definition C.

Let  $X$  be a normed linear vector space,  $X'$  its dual, and  $\{x_n\}$  a sequence in  $X$ . The sequence  $x_n$  is called a weak Cauchy sequence if  $\langle x_n, x' \rangle$  is a Cauchy sequence for every  $x'$  in  $X'$ . We say  $\{x_n\}$  is weakly convergent to  $x$ , written  $x_n \xrightarrow{w} x$ ,  $n \rightarrow \infty$ , if  $\langle x_n, x' \rangle \rightarrow \langle x, x' \rangle$ ,  $n \rightarrow \infty$  for every  $x' \in X'$ .

## APPENDIX

Here, the definition of closed and convex sets and weakly convergent used by this paper are described below (Simmons, 1963, Wouk, 1979).